Universidad del País Vasco Euskal Herriko Unibertsitatea

ZTF-FCT
Zientzia eta Teknologia Fakultatea
Facultad de Ciencia y Tecnología

TRABAJO DE FIN DE GRADO

GRADO EN QUÍMICA

3D BIOPRINTING OF SODIUM ALGINATE HYDROGELS WITH TiO_2 NANOPARTICLES FOR ORGANIC DYE CAPTURE

MEMORIA PRESENTADA POR Sara Muñana González

Fecha de matriculación y defensa: 19/02/2020

Directoras: Leire Ruiz Rubio y Leyre Pérez Álvarez

Departamento: Química Física

INDEX

1 INTRODUCTION

With the development of additive manufacturing technologies, many applications benefited from the faster processing of products without the need for specific tooling.[1] Among the different options for additive manufacturing, 3D bioprinting is an emerging technology that allows the manufacture of complex scaffolds based on a digital design. This technique has been highly improved over the last decade due to increasing interest on tissue engineering and regenerative medicine. It focuses on a layer-by-layer deposition of the so-called bioinks that can vary from polymers, elastomers and hydrogels to biological components such as lipids.

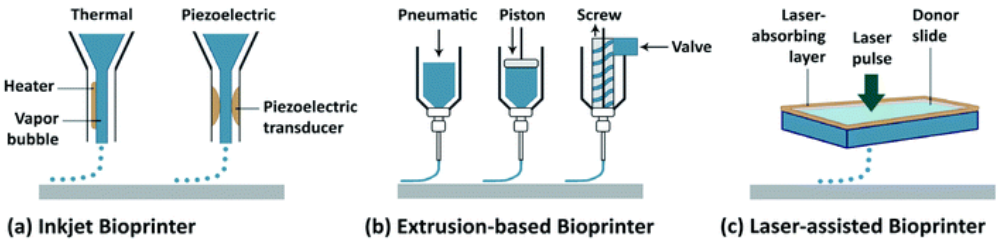

***Figure 1**:* Various types of 3D bioprinting [2]

There are various types of 3D bioprinting methods, such as piezoelectric bioprinting, stereolithography, laser-assisted and pneumatic extrusion (*Figure 1*)[2]. Piezoelectric or thermal injet bioprinting deposits droplets of fluid on a surface and usually presents a resolution of ≈ 100 µm. Even if this method is fast, bioinks with low viscosity are required for a successful printing. Stereolithography constructs a programmed form by selective curing of photopolymerizable bioinks by UV light, and has a resolution of ≈ 1 mm.[3] This is an innovative technique that does not require a surface to work on or a chemical crosslinker; but it does not have very high resolution, and the use of UV light does not make it suitable for cell growth or for the use of natural polymers, since it could lead to cell death or degradation of the polymer. In laser-assisted bioprinting, focused laser pulses cause local vaporization of an energy absorbing layer that leads to the formation of droplets based on the energy and

duration of the pulse. This is a nozzle-less approach that allows printing high viscosity bioinks without facing potential clogging or increasing temperature of ejectors. However, it has some downsides, such as the high cost of the printer or the inability to print large constructs due to the limited width of the laser beam.[4]

The chosen method for this study is the pneumatic extrusion; which deposits a continuous material line on a surface.[5] The bioink is pushed through a nozzle by applying pressure and the resolution depends on the diameter of the printhead, which can go from 15 to 400 µm. This allows to work with more viscous materials, even though cell viability might be penalized due to the high pressures.

The bioink used for this study is sodium alginate (SA). Alginate is a natural polymer extracted from brown algae. It is a linear anionic polysaccharide formed by 1,4-β-d mannuronic acid (M) and α-l guluronic acid (G) units. Often used for micro-organism immobilization and hydrogel synthesis, gelation of alginate occurs rapidly due to electrostatic interactions between the carboxylate groups and divalent or polyvalent cations such as Ca^{2+}, Mn^{2+}, Zn^{2+} and Al^{3+}.[6] Ca^{2+} is the most used cation since its bigger size makes it more suitable for the interaction with multiple carboxylate groups, following the so called “egg-box” model.[7]

The “egg-box” model depends on the orientation of functional groups and the alignment of polymer chains to form a planar 2D structure that surrounds the cation from both sides (*Figure 2*). For this reason, the poly-guluronic acid (GG) units, with their axial connections, favour this type of interaction, as opposed to the equatorial connexions of M units. Therefore, the final cross-linking level of the hydrogel depends on the M/G unit ratio.

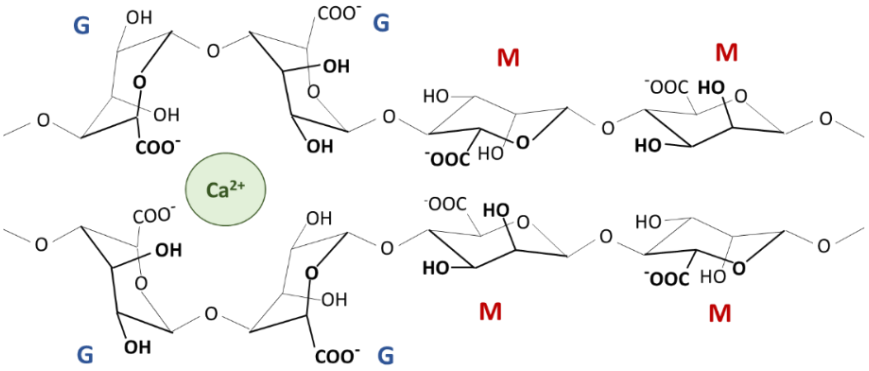

Figure 2: Schematic Ca^{2+} cross-linking of two SA chains following the "egg-box" model

After cross-linking, a water insoluble hydrogel is obtained. Hydrogels are hydrophilic, three-dimensional networks that can absorb large quantities of water or biological fluids. Hydrogel networks can extensively swell in aqueous media.[8] Their hydrophilic nature makes them very useful in tissue engineering, drug delivery, as self-healing materials or for the creation of membranes, among others.

Since it is natural origin product, alginates can be produced at a wide variety of molecular weights (M_W) from 50 to 100000 kDa. Although the G/M unit arrangement can be controlled to some extent during the biosynthesis of the polymer, the final arrangement and MW highly depends on the origin of the source materials.[9] For this reason, in most cases, commercially available sodium alginate powder does not present M_W on the label. Therefore, the most common method to control the stiffness of the final hydrogel product is changing the polymer concentration of the aqueous SA solutions. The increase/decrease of SA content varies the viscosity of the bioink used for 3D printing, which is a very important parameter for pneumatic extrusion based bioprinting. For this reason, an optimization process for the SA concentration and the printing parameters as the one described in this work is necessary when working with natural materials.

In order to change the mechanical, chemical or biological properties of hydrogels, other materials such as ceramics and nanomaterials can be added to the hydrogel matrix. Nanoparticles (NP) are particularly interesting, because, their high surface area to volume ratio gives them new mechanical, chemical, optical and magnetic

properties that are different from those of the bulk material.[10] In this study, TiO_2 nanoparticles are added to the SA hydrogel matrix.

TiO_2 and other metal oxides such as ZnO or Fe_2O_3 are known photosensitive semiconductors that are often used as photocatalysts for oxidation reactions.[11] The photocatalytic properties of TiO_2 are known since the 70s when they were first reported by A. Fujishima in 1972.[12] TiO_2 is a n type semiconductor with a band gap of ≈3eV. For electrons to move from the valence band to the conduction band *hv* must be higher than E_{gap}. For this reason, an artificial UV light source is required for TiO_2 to act as a photocatalyst, since only 3-5% of the sunlight that reaches the troposphere is UV radiation.[13]

TiO_2 photocatalytic reactions mainly proceed via formation of reactive oxygen species (ROS) such as $OH^{\cdot}$, $O_2^{\cdot-}$ and H_2O_2. These hydroxyl radicals can easily oxidize organic contaminants such as dyes. As it can be seen in *Figure 3*, when TiO_2 receives radiation higher than its bandgap energy, it results in the promotion of an electron to the conductive band (e^-_{CB}) and the creation of a hole in the valence band (h^+_{VB}). In contact with water h^+_{VB} produce $OH^{\cdot}$, which has a strong electrophilic nature and can oxidize electron rich molecules. On the other hand, in contact with O_2, e^-_{CB} produce superoxide radical anions ($O_2^{\cdot-}$) whose further reaction with water produces H_2O_2 .[14]

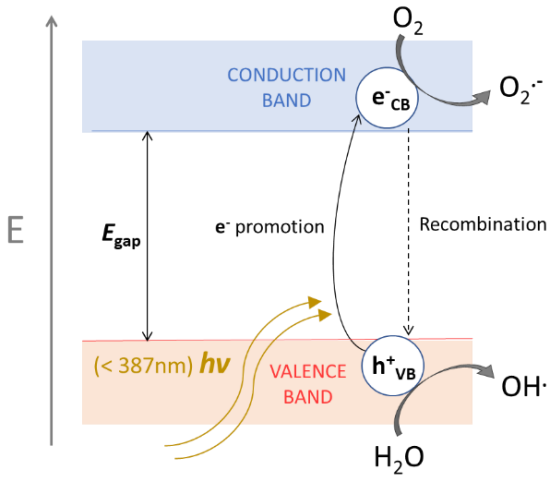

Figure 2: Schematic representation of photocatalytic behaviour of TiO_2

The main application of hydrogels containing TiO_2 NPs studied in this work is the capture and degradation of organic dyes. Often used in textile industry to color fibers and other materials, the presence of dyes in wastewater is very common. If they are not efficiently removed from the environment, they can have a negative impact in the conservation of natural ecosystems. High dye concentration in water can block sunlight, reducing the photosynthetic activity of plants, algae and a wide variety of microorganisms.[15] These compounds can be potentially hazardous for humans as well because of their toxic, mutagenic and carcinogenic nature.[16]

In this study Alizarin Red S (AR), Methylene Blue (MB) and Bromophenol Blue (BPB) dyes have been tested (*Figure 4*).

Alizarin Red S (1,2-dihydroxy-9,10-anthraquinonesulfonic acid) is a water soluble anionic organic dye widely used in textile industry since ancient times.[17] Originally extracted from madder plant roots, it was one of the first natural dyes to be produced synthetically. It also plays an important role in histology and tissue staining, since it can stain calcium deposits in bones.[18]

Methylene blue (tetra-methylthionine chloride) is a water and alcohol soluble cationic thiazine dye commonly used in histology and microbiologic staining.[19] It also plays an important role in medicine as a treatment for methemoglobinemia.[20]

Bromophenol blue 3',3'',5',5''-Tetrabromophenolsulfonephthalein is a laboratory acid-base indicator (color change from yellow to blue at pH 3.0-4.6), an industrial dye and a biological stain. It is commonly used as a size marker for electrophoresis.[21]

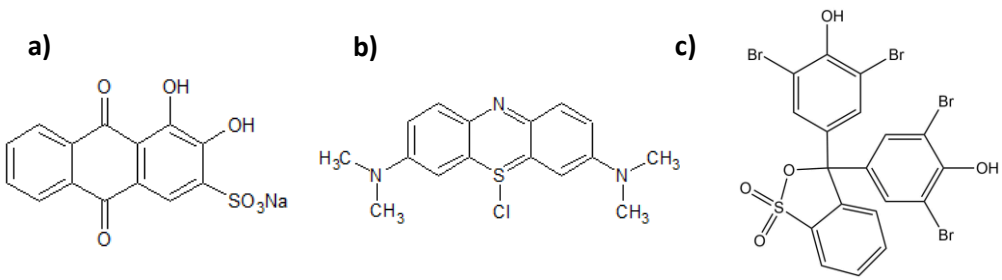

Figure 3: Molecular structures of **a)** Alizarin Red S, **b)** Methylene Blue and **c)** Bromophenol Blue dyes

All these dyes can easily react in presence of reactive oxygen species. The most plausible degradation mechanisms, according to the literature for Alizarin Red, Methylene Blue and Bromophenol Blue are shown in *Schemes 1, 2 and 3* respectively. In all cases the final products are colorless and non-toxic.

In the case of AR, the dye (in a cationic radical form) is attacked at C9 by OH· radicals. This makes the molecule divide in two parts. One part is oxidized to phthalic acid, which is relatively stable. The other part is oxidized to a hydroxyl intermediate and then mineralized to CO_2, H_2O, C and SO_4^{2-} (after going through small organic intermediates such as aldehydes and carboxylic acids). For this reaction to occur, the presence of O_2 is important, because it prevents the recombination of the dye and participates in the formation of more active oxygen radicals.[22]

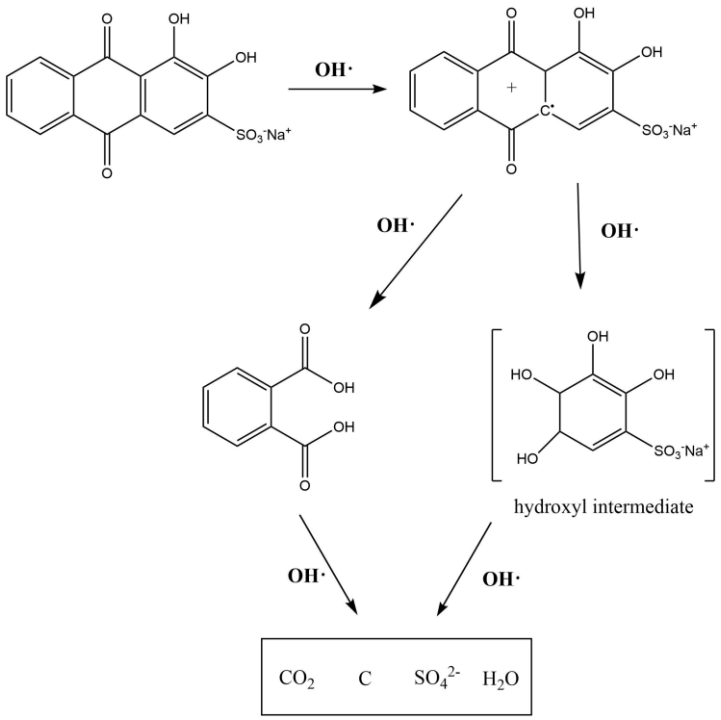

Scheme 1: Degradation pathway for Alizarin Red dye

For MB, the oxygen radical species first attack the N-CH_3 weaker bonds, and the CH_3 groups are further oxidized to formaldehyde or acetic acid. Another OH· attack breaks the C-S and C-N bonds in the middle ring dividing the molecule in two parts (the part containing the -SO_3H group is in equilibrium with phenyl thiophene). Further

oxidation leads to simpler single-ring structures and the final mineralization into inorganic ions.[23]

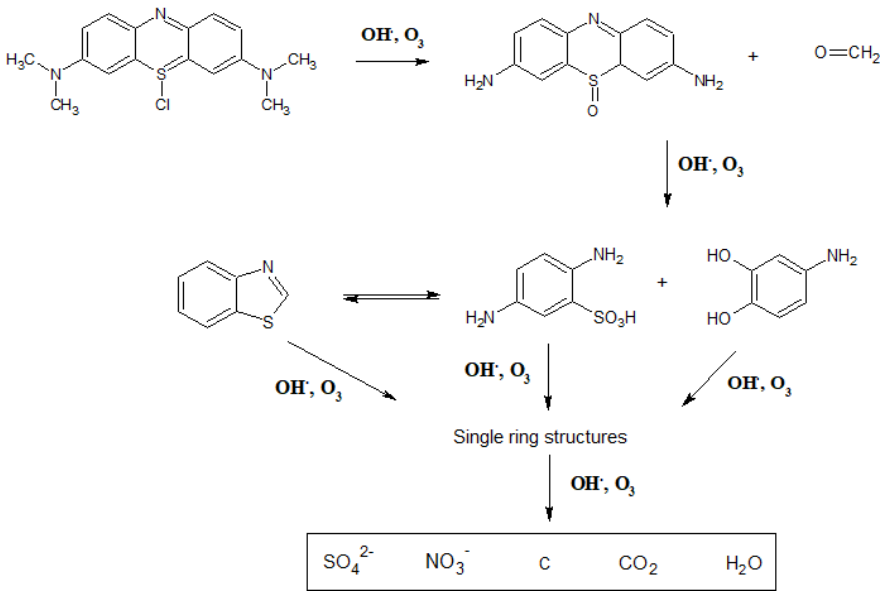

Scheme 2: Degradation pathway for Methylene Blue dye

Finally, BPB, when attacked by the reactive oxygen species, generates 2-hydrosulfonylbenzoic acid and 3, 5-dibromo-4hydroxybenzoic acid as major degradation products. Further degradation through ring opening leads to the formation of aliphatic intermediates and final mineralization into CO_2, H_2O and inorganic ions.[24]

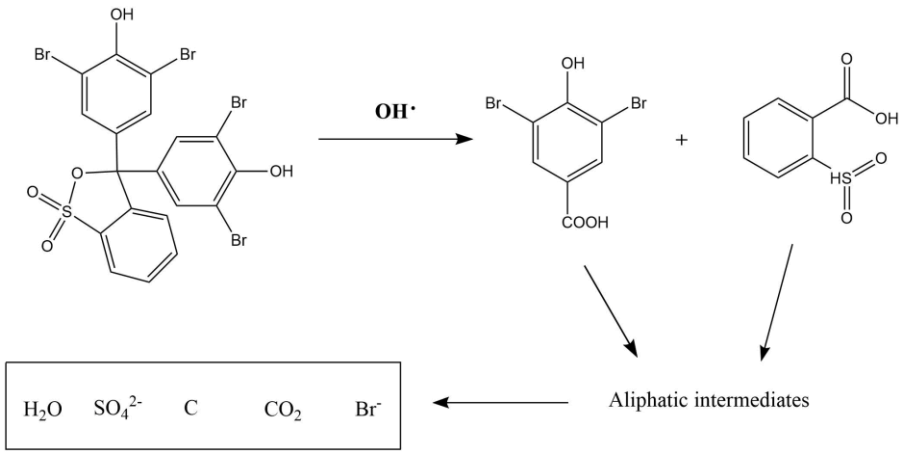

Scheme 3: Degradation pathway for Bromophenol Blue dye

The main goal of this work is to study the printability of SA bioink containing TiO_2 nanoparticles for dye removal, determining the optimum printing parameters for SA concentration, printing speed and pressure. The characterization of the printed hydrogels, as well as the studies on dye absorption will set the bases for the creation of biofriendly SA membranes for capturing organic dyes from industrial wastewaters for their posterior photocatalyzed degradation and elimination.

Photocatalyzed UV degradation of the bioink and the captured dyes will not be covered in this work as it was beyond the scope of this project.

2 MATERIALS AND METHODS

2.1 Materials

Sodium alginate (SA) powder, TiO_2 nanopowder (<100nm particle size, 99.5% pure) and Alizarin Red S dye powder were purchased from Sigma Aldrich, St Louis, MO, USA. $CaCl_2$ used for crosslinking and Methylene Blue dye (Kühne solution for microscopy) were purchased from Panreac, Madrid, Spain. Bromophenol Blue dye powder was purchased from Doesder, Barcelona, Spain.

2.2 Bioinnk preparation

40 mL of 10% (w/w) SA solution were prepared using deionized water and mechanically stirred overnight. Then, an aqueous dispersion of TiO_2 nanoparticles (10 mL) was added, followed by 3-4 h more of mechanical stirring, obtaining a homogeneous mixture. The same procedure was followed to prepare three 10% SA sample solutions (containing 0%, 0.1% and 0.5% of TiO_2 NPs), three sample solutions of 7.5% SA and other three of 5% SA.

2.3 3D Bioprinting optimization

The resulting bioinks were printed in a 3D bioprinter (Inkredible+, Cellink) on a glass Petri dish previously wet with a 1M $CaCl_2$ solution. The printing was carried out at

room temperature using a pneumatic print head with a 25 G (0.254 mm diameter) nozzle. The nozzle-base distance was set at 7.4 mm.

Prior to printing, the viscosity of each solution was measured with a Brookfield Ametek DV2T viscosimeter using a number 6 spindle.

2.4 Characterization of hydrogels

Thermal degradation of hydrogels was studied by thermogravimetric analysis (TGA/SDTA851^e, Mettler Toledo) after crosslinking for 24 h and freeze-dried for 12 h. Samples of 15 mg were heated under nitrogen atmosphere (flow of 20 mL/min) at a 5 ^oC/min heating rate from 25 to 800 ^oC.

The Young modulus of the hydrogel lines was determined by a tension test in a universal testing machine (Metrotec, TLS) at 5 mm/min test speed.

2.5 Swelling

Hydrogel 2x2 cm grids printed at optimized conditions were freeze dried for 12 h after 24 h crosslinking with $CaCl_2$ 1M solution. 3-4 grids were used for each swelling test. The scaffolds were introduced in deionized water at pH 7.6 and weighted at certain time intervals.

2.6 Study of dye absorption and reactivity

One 2x2cm grid, previously crosslinked and freeze-dried was introduced in each vial containing dilutions in water of Methylene Blue (MB), Alizarin Red (AR) and Bromophenol Blue (BPB) dyes respectively for 24h for the qualitative study of hydrogel-dye interactions.

For the study of the reactivity of AR five vials containing 50 ppm AR solution in deionized water were prepared. Different samples of ≈ 20 mg of SA polymer (Vial A), 10% SA 0% TiO_2 NP hydrogels (Vial B), 10% SA 0.5% TiO_2 NP hydrogels (Vial C) and TiO_2 nanoparticles (Vial D) were introduced in the solutions for 24h.

The quantification of dye absorption was studied by UV-Vis spectrophotometry using MB dye and a Cintra 303 GBC spectrophotometer. The calibration curve was built

measuring the maximum absorbance of MB aqueous solutions at known concentrations ranging from 0 to 20 ppm. For the kinetic study, 10 dried grids of 10% SA 0% TiO_2 NP were introduced in a 15 ppm MB solution and the absorbance of the solution was measured at certain time intervals. The same procedure was followed using the 10% SA 0.5% TiO_2 NP hydrogels.

3 RESULTS AND DISCUSSION

3.1 3D Bioprinting optimization

In order to determine the optimum pressure and printing speed values for the 3D printing of SA-TiO_2NP hydrogels, 3 lines were printed at a fixed pressure at 300, 600 and 800 mm/min printing speed. Each test was repeated 4-5 times to ensure that the results were constant.

Each set of 3 lines was photographed, and lines were evaluated in terms of homogeneity and thickness. The images were analyzed with programme Image J to determine the diameter of the hydrogel lines. 5 measurements were taken for each line.

Then, the lines were marked as red if they showed very poor homogeneity and/or had a diameter of > 1.0 mm; yellow if they showed an overall good homogeneity with small bumps or thickness changes along the line with a line diameter of 0.6 to 1.0 mm; and green if they were thin homogeneous lines with a diameter of < 0.6 mm. An example containing these three types of hydrogel lines can be observed in *Figure 5*.

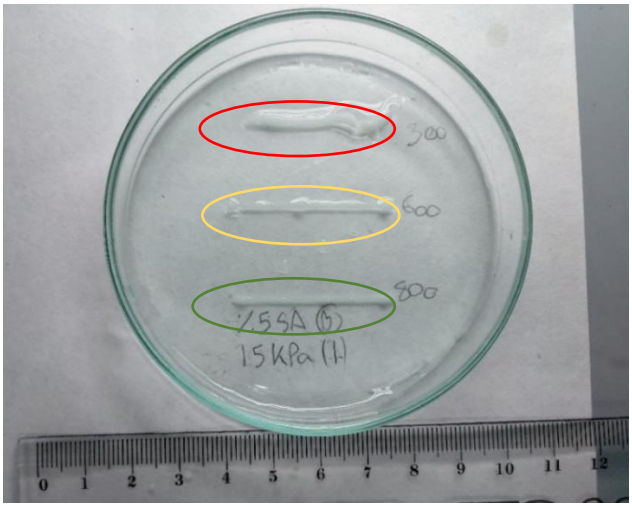

Figure 5: Hydrogel lines with 5% SA and 0.5% NP printed at 15 kPa pressure. Red circle indicates a poorly homogenous line, yellow indicates a mediocre line and green a thin homogenous line

After the analysis of the size and homogeneity of the lines, it was determined that the 5% SA solutions were not viscous enough for an optimum printing ($\mu < 1000$ cP in both cases). Although some of the lines printed using these solutions were uniform, they were mostly too thick, and some drops leaked between the lines due to the low viscosity. This phenomenon can be observed in *Figure 6* a), b) and c).

Even though the leaking was not as evident in the 5% SA solutions containing 0.5% TiO_2 NPs (*Figure 6* d), e) and f)), it still occurred. Also, despite some of the lines printed at 600 and 800 mm/min were relatively thin and homogeneous, in comparison with the 10% SA and 7.5% SA samples, the diameter of the lines was large. Therefor, the %5 SA solutions were not used to print the hydrogels that were later characterized. The thinnest 5% SA 0% NPs hydrogel was printed at 20 kPa pressure and 800 mm/min speed and had a diameter of 0.9 ± 0.1 mm. The thinnest 5% SA 0.5% NPs hydrogel was printed at 10 kPa pressure and 800 mm/min speed and had a diameter of 0.81 ± 0.06 mm.

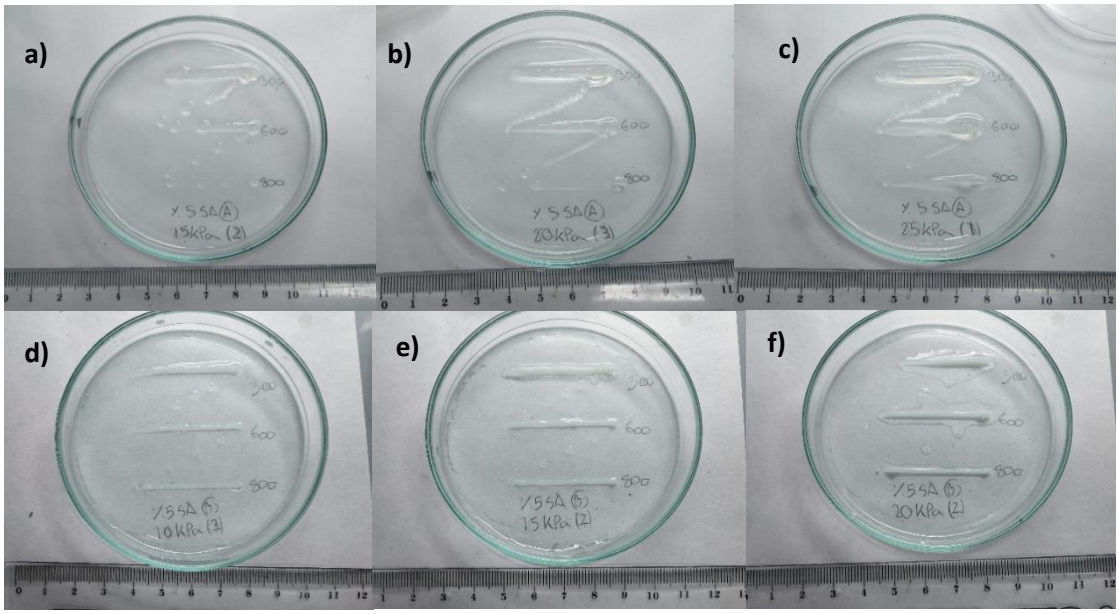

Figure 6: 5% SA 0% TiO_2 NPs hydrogel lines printed at **a)** 15 kPa **b)** 20 kPa and **c)** 25 kPa. 5% SA 0.5% TiO_2 NPs hydrogel lines printed at **d)** 10 kPa **e)** 15 kPa and **f)** 20 kPa

The 7.5% SA solutions had a greater viscosity, ranging from 3500 to 4600 cP. Due to the increase of the viscosity, no leaking was observed between the printed lines. The solutions containing TiO_2 NPs were more viscous, so higher pressure values were required for optimum printing.

The thinnest 7.5% SA 0% NPs hydrogel was printed at 30 kPa pressure and 800 mm/min speed and had a diameter of 0.50 ± 0.03 mm (*Figure 7* a)). The thinnest 7.5% SA 0.1% NPs hydrogel was printed at 30 kPa pressure and 800 mm/min speed and had a diameter of 0.52 ± 0.04 mm (*Figure 7* b)). The thinnest 7.5% SA 0.5% NPs hydrogel was printed at 30 kPa pressure and 800 mm/min speed and had a diameter of 0.49 ± 0.03 mm (*Figure 7* c)).

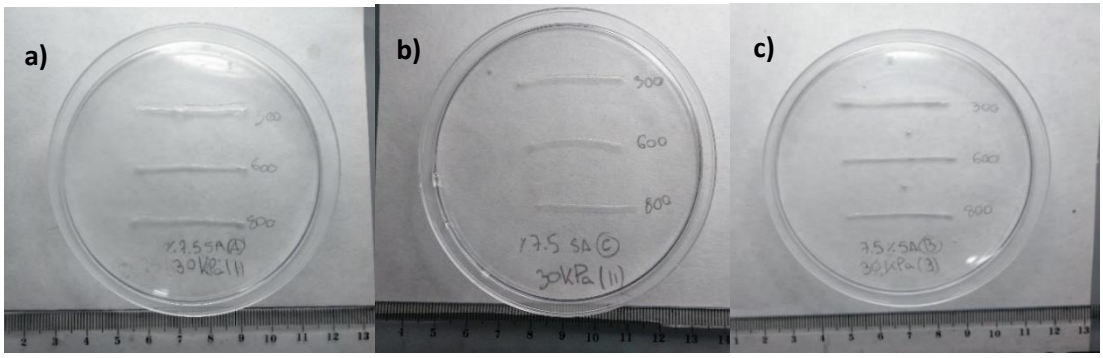

Figure 7: **a)** 7.5% SA 0% TiO_2 NPs **b)** 7.5% SA 0.1% TiO_2 NPs and **c)** 7.5% SA 0.5% TiO_2 NPs hydrogel lines printed at 30 kPa pressure

The 10% SA samples were the most viscous among the tested solutions, having a viscosity ranging from 8300 to 13500 cP. No leaking was observed between the printed lines. However, despite the increase of the viscosity in comparison to the 7.5% SA samples, the pressure values required for optimum printing were similar.

The thinnest 10% SA 0% NPs hydrogel was printed at 25 kPa pressure and 800 mm/min speed and had a diameter of 0.45 ± 0.05 mm (*Figure 8* a)). The thinnest 10 % SA 0.1% NPs hydrogel was printed at 35 kPa pressure and 800 mm/min speed and had a diameter of 0.38 ± 0.01 mm (*Figure 8* b)). The thinnest 10% SA 0.5% NPs hydrogel was printed at 35 kPa pressure and 800 mm/min speed and had a diameter 0.51 ± 0.07 mm (*Figure 8* c)).

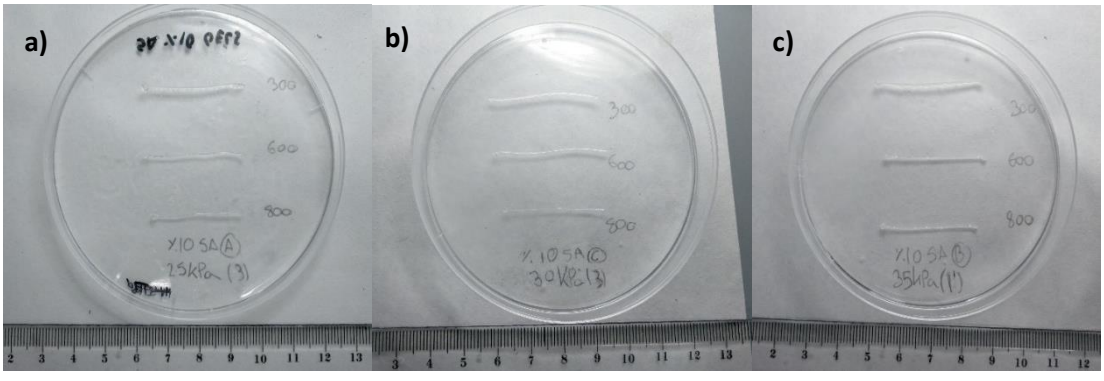

Figure 8**: a)** 10% SA 0% TiO_2 NPs hydrogels printed at 25 kPa pressure, **b)** 10% SA 0.1% TiO_2 NPs hydrogels printed at 30 kPa pressure and **c)** 10% SA 0.5% TiO_2 NPs hydrogels printed at 35 kPa pressure

A summary of the optimized printing parameters for each SA solution can be observed in *Table 1*. As expected, the increase of SA concentration augmented the viscosity of the solutions and, therefore, the pressure required for an optimum printing. The addition of TiO_2 NPs also caused an increase in the viscosity of the solutions and the optimum printing pressure. It was determined that in order to have a line diameter of < 0.6 mm the bioink should have a viscosity of > 3000 cP.

Table 1: Optimized printing parameters for tested SA solutions

Solution	Viscosity (cP)	Optimum P (kPa)	Optimum speed (mm/min)	Line thickness (mm)	Reference image
5% SA 0% NP	666	20	800	0.9 ± 0.1	Figure 5 b)
5% SA 0.5% NP	740	10	800	0.81 ± 0.06	Figure 5 d)
7.5% SA 0% NP	3500	30	800	0.50 ± 0.03	Figure 6 a)
7.5% SA 0.1% NP	4500	30	800	0.52 ± 0.04	Figure 6 b)
7.5% SA 0.5% NP	4600	30	800	0.49 ± 0.03	Figure 6 c)
10% SA 0% NP	8650	25	800	0.45 ± 0.05	Figure 7 a)
10% SA 0.1% NP	11000	30	800	0.38 ± 0.01	Figure 7 b)
10% SA 0.5% NP	13500	35	800	0.51 ± 0.07	Figure 7 c)

3.2 Thermogravimetric analysis (TGA)

The thermal stability of the bioinks was analyzed by TGA. The thermographs obtained for previously dried hydrogels of 10% SA 0%, 0.1% and 0.5% TiO_2 NPs are depicted in *Figures 9*, *10* and *11* respectively.

The degradation of the three samples was very similar, presenting two main degradation steps of 15% and 7% occurring at T = 158-178 ^{o}C (T_{peak} = 168 ^{o}C) and T = 278-301 ^{o}C (T_{peak} = 290 ^{o}C) respectively. For all 10% SA 0%, 0.1% and 0.5% TiO2 NP samples the high final residue of 40%, 42% and 39% respectively matches the degradation profile of a typical polysaccharide. Even if, the presence of TiO_2 NPs could vary the degradation pathways due to catalytic effects, in these systems this influence was not observed, so these NPs concentrations do not seem to affect the degradation of the hydrogel. It was expected to find small changes on the final

residue corresponding to the NPs concentration. However, the amount of NPs in the gels was too small to get any noticeable difference.

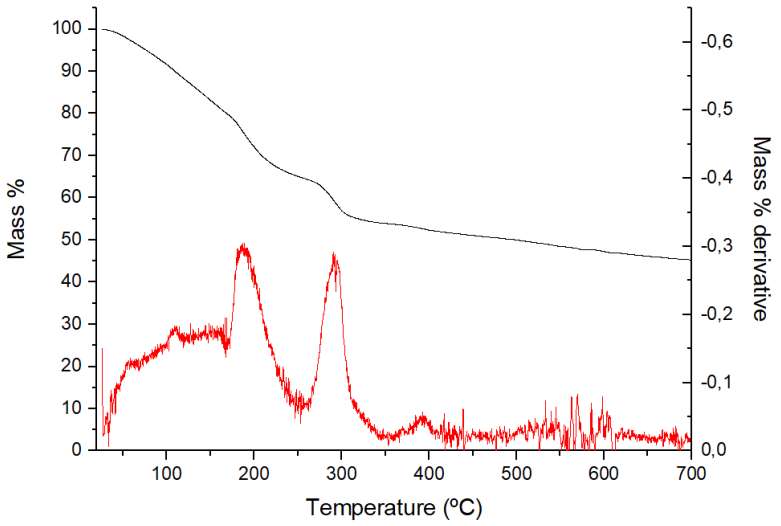

Figure 9: TGA-DTA analysis of 10% SA 0% TiO_2 NPs hydrogels

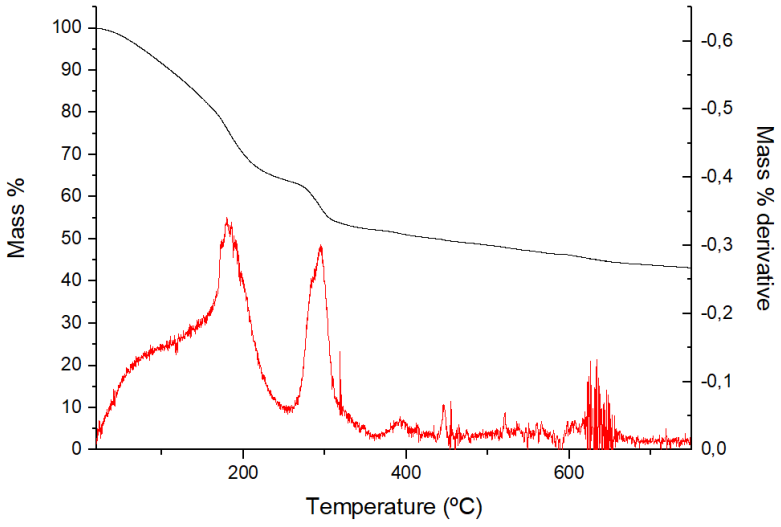

Figure 10: TGA-DTA analysis of 10% SA 0.1% TiO_2 NPs hydrogels

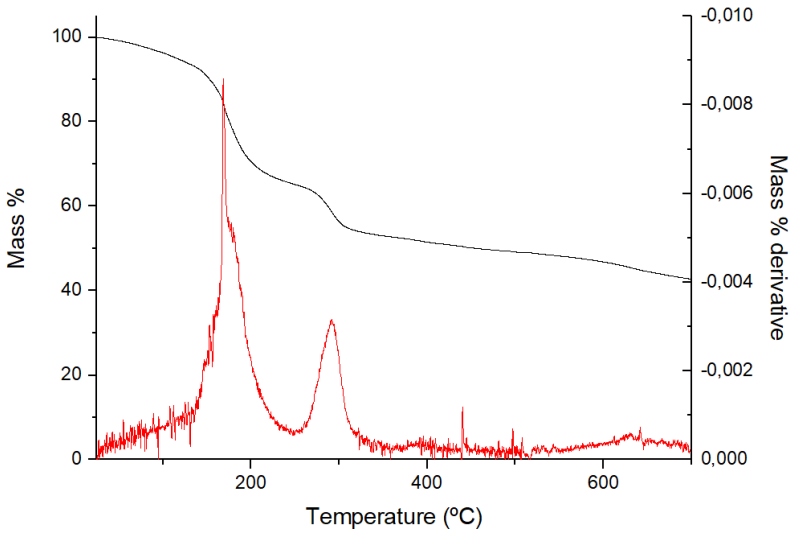

***Figure 11**:* TGA-DTA analysis of 10% SA 0.5% TiO_2 NPs hydrogels

3.3 Mechanical properties

For the study of the mechanical properties a tension test was carried out for 10% SA 0%, 0.1% and 0.5% TiO_2 NP hydrogel lines. The obtained stress (σ) vs. strain (ε) representation can be observed in *Figure 12*. The Young's Modulus (*E*) of the hydrogel samples was determined from the slope of the stress vs. strain curve at < 0.1 strain levels (*1*).

$$\sigma = E \cdot \varepsilon \qquad (1)$$

The test was repeated 5 times for each composition, obtaining an average Young's Modulus value of 4 ± 1 MPa for 10% SA 0% TiO_2 NPs hydrogels, 6 ± 1 MPa for 10% SA 0.1% TiO_2 NPs and 7 ± 1 MPa for 10% SA 0.5% TiO_2 NPs. In this case, the addition of nanoparticles had a positive impact on the stiffness of the hydrogels.

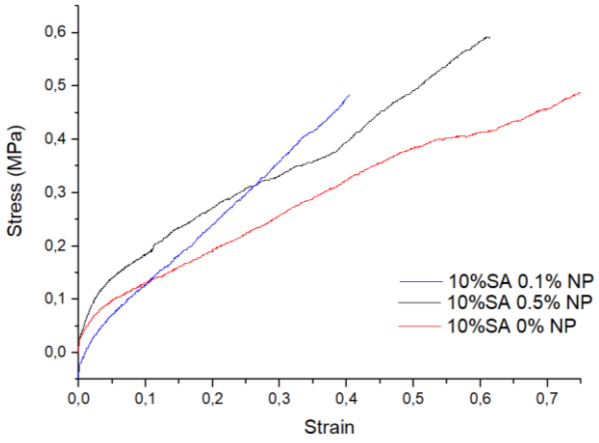

***Figure 12**:* Strain vs. stress representation of the mechanical properties for 10% SA 0%, 0.1% and 0.5% NPs hydrogels.

3.4 Swelling

Freeze-dried hydrogel grids were introduced in deionized water at pH 7.6 ,and weighted at 1 min time interval from t_0 to t = 5 min, and 5 min time interval from t = 5 min to t = 40 min. The experiment was repeated three times using gels with the same NPs content.

The swelling ratio of the hydrogels was determined by comparing the weight of the hydrogel at each time with the initial weight of the dried hydrogels (*2*).

$$\text{Swelling } \%(t) = \frac{\text{Hydrogel mass (t)}}{\text{Hydrogel mass } (t_0)} \cdot 100 \qquad (2)$$

As seen on *Figure 13*, 10% SA 0% NPs hydrogels swelled untill 460% of their weight at t = 1 min. After releasing the excess of water, the swelling remained constant at 420-430% of the initial weight.

A similar behaviour, but in a smaller scale, was observed in the 10% SA 0.5% NPs samples, which swelled untill 320% of the initial weight at t = 1 min and then reamined constant at 270-280% after releasing the excess of water.

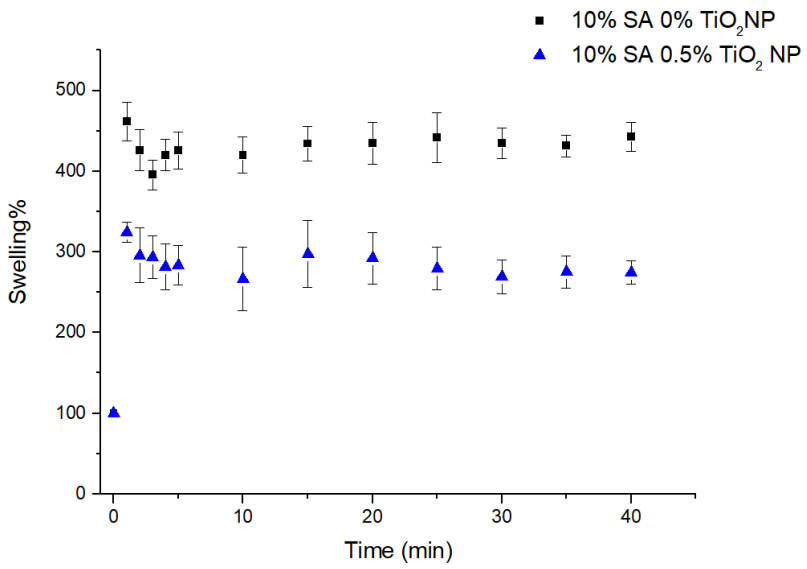

Figure 13: Swelling ratio of 10% SA 0% and 0.5% TiO_2 NP hydrogels

A possible explanation for this behaviour is that at t = 1 min water molecules, apart from filling the empty cavities of the gel also replaced some of the Ca^{2+} ions, making it swell more. But since Ca^{2+} ions have more affinity with alginate chains than water molecules, they were rapidly replaced back, leading to the mass loss.

It was expected that the hydrogels containing NPs would swell less than the ones without NPs, because, the interactions between the NPs and the hydrogel can lead to a reduction of the pore size.

3.5 Qualitative studies on dye absorption and reactivity

After 24h in their respective solutions, the 10% SA 0% TiO_2 NP grids were compared in terms of color intensity in order to find the most suitable dye for the absorption kinetics experiment. As it can be observed in *Figure 14*, the grids in contact with MB and AR dyes present an intense color in comparison with the blank sample, showing strong interaction between hydrogels and dyes. On the other hand, the hydrogel sample in contact with BPB dye shows an almost imperceptible change in color. When comparing the chemical structures of the dyes, one possible explanation is that the BPB molecule, being bigger than the other two (it is a three-dimensional molecule

with 4 rings, while the others are almost planar and consist of just 3 rings) does not have the size to fit into the cavities of the gel.

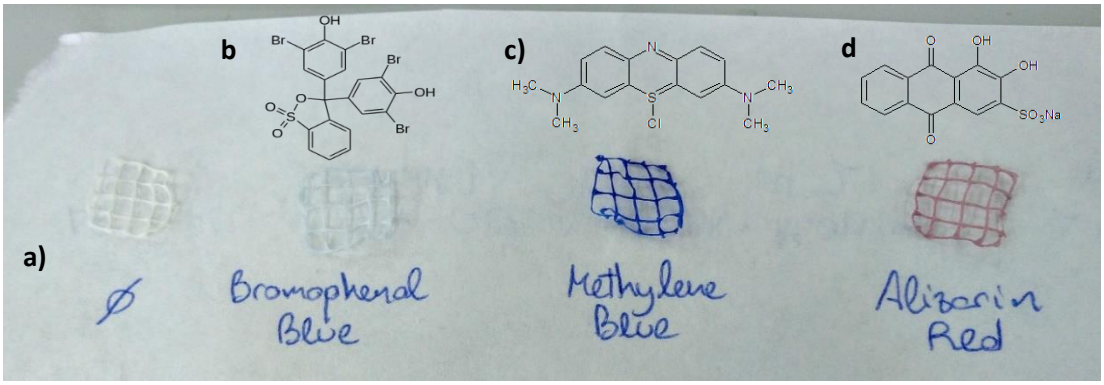

Figure 14: 10% SA 0% TiO_2 NP hydrogel grids after 24 h in **a)** deionized water, and aqueous solutions of **b)** BPB, **c)** MB and **d)** AR dyes with their respective chemical structures

Another phenomenon that occurred during this experiment was the formation of a red precipitate on the AR sample, that adsorbed on the surface of the hydrogel giving it that color. The main hypothesis is that this precipitate is the calcium salt observed in *Figure 15* which is a product formed when AR is in contact with calcium deposits by electrostatic interaction between Ca^{2+} and the deprotonated -OH groups of AR. [17] This reaction might have occurred in contact with the hydrogel because $CaCl_2$ was previously used as a cross-linker.

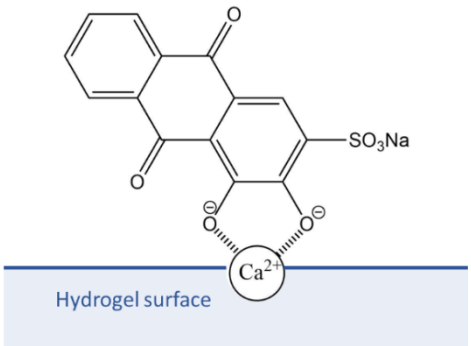

Figure 15: Possible AR-Ca^{2+} salt structure

In order to check if the calcium within the hydrogels was the only compound AR could react with, 5 vials containing SA polymer (A), 10% SA 0% TiO_2 NP hydrogel grids (B), 10% SA 0.5% TiO_2 NP hydrogel grids (C), TiO_2 nanopowder (D) and a blank were

prepared and an aqueous solution of 50 ppm of AR was added to each vial. After 24 h, the vial containing TiO_2 nanopowder (*Figure 16 d)*) and the blank showed no sign of reaction; but, the vials containing vials containing SA polymer, 10% SA 0% TiO_2 NP hydrogel grids and 10% SA 0.5% TiO_2 NP hydrogel grids (*Figure 16 a), b) and c)*) had reacted: the solution containing the polymer turned red and in the samples containing hydrogels a red precipitate appeared. So, it was determined that AR also reacted in contact with sodium alginate.

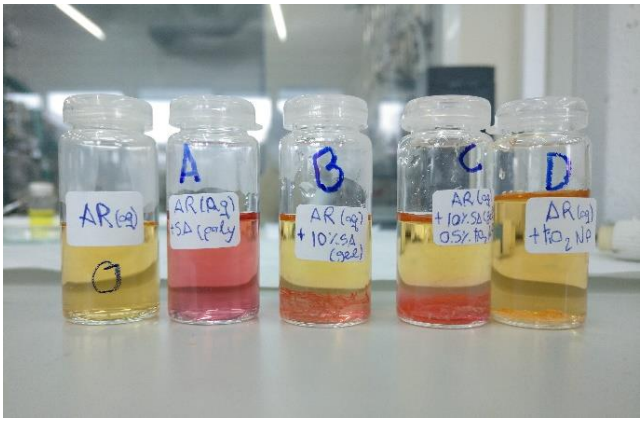

***Figure 16**: Qualitative study on the reactivity of AR after 24 h*

After the qualitative experiments, it was determined that, due to the reactivity of AR and the size and poor affinity with the hydrogels of BPB, the most adequate dye to perform quantitative dye absorption experiments was MB.

3.6 Dye absorption kinetics

The UV-vis spectra of diluted MB dye was obtained to determine the maximum absorbance wavelength (*Figure 17*). The maximum absorbance peak was found to be at 663 nm. A calibration curve was built by measuring the absorbance at 669 nm of 5 aqueous MB solutions with known concentrations ranging from 0 to 20 ppm. The concentration of MB was determined by measuring the absorbance at the wavelength of 669 nm following Beer-Lambert's law *(3)* and compared with its calibration curve both in deionized water (A = 0.143 L/mg + 0.006; R^2 = 0.995).

$$A = \varepsilon \cdot l \cdot [MB] \qquad (3)$$

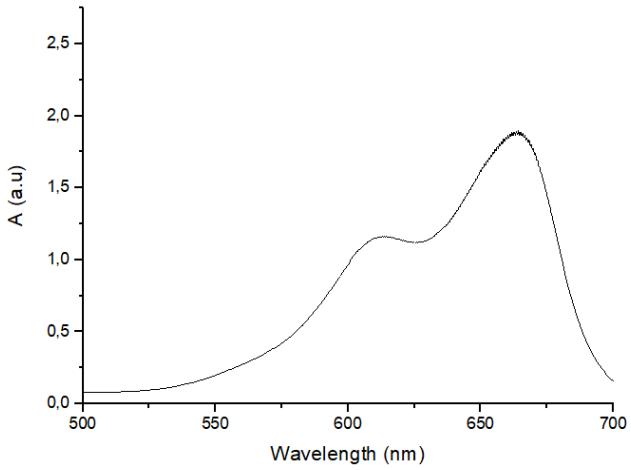

Figure 17: UV-vis spectrum of MB dye

The dye absorption test was carried out by sumerging 10 hydrogel grids in a 15.8 ppm MB solution and measuring the absorbance at t = 2 min, t = 5 min, time intervals of 5 min from t = 5 min to t = 30 min and finally t = 40 min, t = 60 min and t = 90 min. The [MB] absorbed in the gels was determined by difference between the initial concentration of the solution and the MB concentration at t, assuming that the dye that was not in the solution was loaded in the hydrogels. The $[MB]_{Hydrogel}$ change over the time can be seen in *Figure 18* for both 10% SA 0% NP and 10% SA 0.5% NP samples. The results show that the hydrogels absorbed 4.1 ppm of MB in 90 minutes meaning they captured 26% of the initial dye concentration. Both samples showed very similar behaviour. The decrease in concentration followed an almost linear tendency in the first 30 minutes and it slowed down as it got closer to the saturation point.

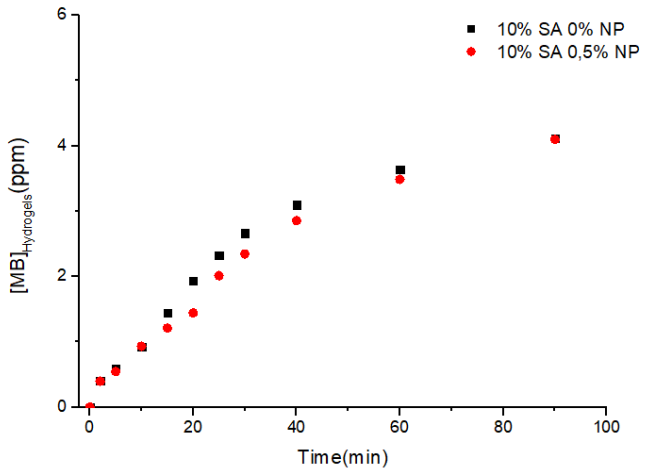

Figure 18: Variation of $[MB]_{Hydrogels}$ over time in 10% SA 0% and 0.5% TiO_2 NPs hydrogels

Another measurement was taken at t = 24 h to see the final concentration in the solution assuming that the gel would have reached the saturation point at that time. After 24 h the [MB] loaded in the hydrogels was 6.1 ppm for the 10% SA 0% NP sample and 6.0 ppm for the 10% SA 0.5% NP sample, meaning a final MB capture of 42% relative to the initial concentration. These results show that, despite the relative thinness of the printed hydrogel grids that does not allow to have a lot of space within the gels for the dye to fit in, a quantifiable amount of dye was captured. During the process the hydrogel grids did not react with the dye and no sign of degradation of the hydrogels was observed.

4 CONCLUSIONS

In summary, 3D printing parameters were optimized for the sodium alginate bioinks with different polymer and TiO_2 nanoparticle concentrations. The aqueous alginate solutions were printable at all tested nanoparticle concentrations and the optimum pressure values for printing changed depending on the viscosity of the solution, being the more viscous solutions of 7.5% and 10% alginate concentration the most adequate bioinks for an optimum bioprinting. The addition of TiO_2 nanoparticles does not affect the printability of the bioinks at concentrations below 0.5%, although the

interactions between the polymer chains and the nanoparticles cause small alterations on the viscosity.

The tests showed that the interaction between the TiO_2 nanoparticles and the polymer does not affect the thermal degradation of the hydrogels. The Young's modulus obtained from mechanical tests increases due to the rigidity provided by the intercalation of the TiO_2 nanoparticles in the polymer chains.

As the pore size of the hydrogel determines the diffusion of the dyes within the hydrogel network, the dye absorbing capacity of the hydrogel depends on its structure. Due to the pore size of the bioprinted hydrogels, the size bigger of the Bromophenol Blue dye molecules limited its diffusion and Alizarin Red reacted with the Ca^{2+} cross-linked hydrogels producing a red precipitate. Methylene blue has a higher diffusion within the hydrogel network that allows a successful, quantifiable capture of the dye.

Due to time and equipment limitations photocatalyzed degradation of the dyes within the gels was not tested, but it is the main goal of further research on this topic.

5 BIBLIOGRAPHY

[1] S. Bose et al. *Materials Today* (**2013**) 16, 12 496-504

[2] P. Selcan Gungor-Ozkerim et al. *Biomater. Sci.* (**2018**) 6, 915-946

[3] Jia Min Lee, Wai Yee Yeong; *Adv. Healthcare Mater.* (**2016**) 5, 2856–2865

[4] Ahu Arslan-Yildiz et al. *Biofabrication* (**2016**) 8, 014103

[5] B. Duan, et al*. J. Biomed. Mater. Res. A.* (**2013**) 101, 1255.

[6] S. Winkler, D. L. Kaplan; *Biosynthesized Materials: Properties and Processing,* in *Encyclopedia of Materials: Science and Technology,* Elsevier Science Ltd (**2001**) 609-615

[7] P. M. Bedê, et al. *Polímeros*, (2017) 27(4), 267-272

[8] Qinyuan Chai et al.; *Gels* (**2017**) 3, 6 1-15

[9] A. D. Augst et al.; *Macromol. Biosci*. (**2006**) 6, 623–633

[10] I. Khan et al.; *Arabian Journal of Chemistry* (**2019**) 12, 908–931

[11] M. L. de Souza, P. Corio; *Applied Catalysis B: Environmental* (**2013**) 136, 325-333

[12] A. Fujishima et al. *Nature* (**1972**) 238, 37-38

[13] C. H. Nguyen et al. *Separation and Purification Technology* 232 (**2019**) 115962

[14] M. Umar, H. A. Aziz; *Photocatalytic Degradation of Organic Pollutants in Water,* in *Organic Pollutants - Monitoring, Risk and Treatment* (**2013**) 8 196-208

[15] S. K. Kansal et al. *Materials Letters* (**2013**) 106, 385-389

[16] M. Albert et al. *J Pediatr Surg* (**2003**) 38, 1244-1245

[17] National Center for Biotechnology Information. PubChem Database. Alizarin, CID=6293, https://pubchem.ncbi.nlm.nih.gov/compound/Alizarin (accessed on Jan. 19, 2020)

[18] Moriguchi et al. *Journal of Colloid and Interface Science* (**2003**) 260, 19–25

[19] National Center for Biotechnology Information. PubChem Database. Methylene blue, CID=6099, https://pubchem.ncbi.nlm.nih.gov/compound/Methylene-blue (accessed on Jan. 20, 2020)

[20] Drugbank database. Methylene blue, DB09241, https://www.drugbank.ca/drugs/DB09241 (accessed on Jan. 20, 2020)

[21] National Center for Biotechnology Information. PubChem Database. Bromophenol blue, CID=8272, https://pubchem.ncbi.nlm.nih.gov/compound/Bromophenol-blue (accessed on Jan. 20, 2020)

[22] G. Liu et al. *Journal of Molecular Catalysis A: Chemical* (**2000**) 153, 221–229

[23] F. Huang et al. *Chemical Engineering Journal* (**2010**) 162, 250–256

[24] J. Hong et al. *Desalination* (**2007**) 214, 62–69